RFID-based Endoleak Detection by Dissolvable Antennas and Auto-Tuning IC

Federica Naccarata
Pervasive Electromagnetics Lab
University of Rome Tor Vergata
Rome, Italy
naccarata@ing.uniroma2.it

Marco Di Cristofano
University of Rome Tor Vergata
Rome, Italy
marco.dicristofano@alumni.uniroma2.eu

Gaetano Marrocco
Pervasive Electromagnetics Lab
University of Rome Tor Vergata
Rome, Italy
gaetano.marrocco@uniroma2.it

***Abstract*—Endoleak is one of the major complications after surgery to treat abdominal aneurysms. It is characterized by blood flow outside the stent graft within the aneurysm sac, leading to increased pressure with a concomitant risk of rupture of the sac itself. As standard screenings are operator-dependent and intrusive, this paper proposes a battery-less method to wirelessly monitor the presence of endoleak-related blood flow. The unobtrusive sensing element is an antenna, equipped with an auto-tuning RFID IC and a portion of bioresorbable coating, placed proximally to the stent and inside the aneurysm sac. The presence of liquid blood induces the hydrolysis of the bioresorbable coating, leading to the exposure of part of the antenna to the biological environment. The variation of the antenna boundary condition is detected by the aforementioned IC giving threshold levels following over time the phenomenon evolution. Numerical simulations and a preliminary experiment demonstrate the robust communication link and the feasibility of the sensing mechanism.**

***Index Terms*—Radio Frequency Identification, Bioresorbable Coating, Endoleak Detection, Wireless Monitoring**

I. Introduction

Aortic abdominal aneurysms are generally treated surgically by endovascular aortic repair (EVAR) [1], when the diameter of the aneurysm is > 5.5 cm, as there is a high risk of rupture [2]. EVAR is a minimally invasive surgical procedure that requires a catheter to insert a stent graft to stabilize the aneurysm by its exclusion from the circulatory system. A common complication following EVAR is the endoleak with an incidence up to 45% [3] with significant morbidity and mortality. The endoleak involves the flow of blood outside the stent graft within the aneurysm sac, leading to an increase in pressure. Consequently, endotension leads to an enlargement of the sac with a concomitant risk of rupture. Furthermore, blood flow interferes with the formation of an organized thrombus that facilitates aneurysm shrinkage. The causes of endoleak can be numerous, including detachment of the distal portion of the graft, a defect in the graft itself such as fabric tear/porosity, or a retrograde flow into the sac from aortic side branches [4].

Currently, long-term follow-up after EVAR includes contrast-enhanced ultrasound and computed tomography angiography [5]. Unfortunately, these tests cannot be performed frequently enough to promptly detect endoleaks, due to the high doses of radiation and chemical agents.

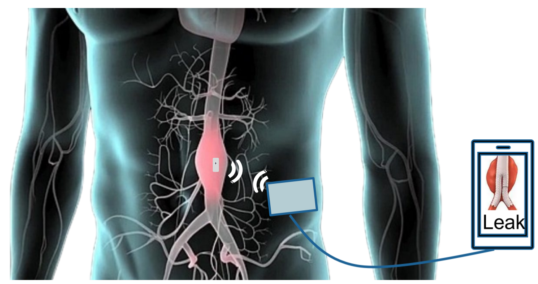

Fig. 1. Concept of RFID-based endoleak monitoring.

An alternative diagnostic strategy based on *in-situ* sensors and wireless connectivity could offer a clearer picture of the sequence of events that occur inside the aneurysm, after surgical treatment, for the early detection of endoleaks, thus improving life expectancy.

In [6] the helicoidal steel wires of the stent are exploited as an antenna to establish a communication link for biotelemetry purposes. Wireless communication and detection capabilities are demonstrated with a blood flow voltage-based sensor [7] and a PCB with multiple pressure sensors [8] mounted on the graft. However, there are several additional elements wrapped around the stent with non-negligible design complexity. In this scenario, Radio Frequency Identification (RFID) technology in the UHF band ($860 - 960$ MHz) enables the miniaturization of the sensor and reduces the amount of required electronics. For example, several implanted medical devices such as aortic valve prostheses [9], [10], stent [11], hip prostheses [12], and dental implants [13] were augmented with sensing and communication capabilities.

This paper, exploring a different approach, exploits a new generation of RFID integrated circuits (ICs) [14] provided with auto-tuning capability, i.e. it automatically modifies its susceptance to match with the hosting antenna in case of different local boundary conditions, and a bioresorbable coating over a portion of the implanted antenna to detect endoleak. The leading idea (Fig. 1) is to insert an unobtrusive sensing element, i.e. the antenna itself, placed proximally to the stent and inside the aneurysm sac. This device can be anchored to the stent since it is located inside the aneurysm sac and therefore does not obstruct the dynamic flow of blood within the aortic vessel. The occurrence of endoleak-related blood flow is identified by a threshold sensing mechanism, where over time the bioresorbable coating is degraded by hydrolysis upon contact with liquid blood. Such blood, hence, replaces the dry tissue of the thrombus and indicates the presence of endoleak. This implies that the antenna has portions exposed to the biological environment; thus a variation in its boundary conditions can be detected by using the aforementioned RFID ICs.

II. Rationale of Sensing by Auto-Tuning IC

The selected IC is the Magnus-S3 by Axzon [14] equipped with auto-tuning technology, having nominal input admittance $Y_{IC} = 0.6 + i15.7\ mS$ at 900 MHz and power sensitivity $P_{IC} = -13.6$ dBm. The core of the auto-tuning RFID IC can be modeled by resistance in parallel to an adaptive internal network of parallel capacitors, whose total capacitance depends on the number of activated capacitors [15]:

$$C_{IC} = C_{min} + sC_{step} \tag{1}$$

ranging from a minimum value C_{min} to a maximum value with incremental step C_{step} in the linear range. Following an RFID query, the IC returns the integer number s, hereafter referred to as *sensor code*. The variable susceptance of the IC is derived by imposing the auto-tuning condition

$$|B_{IC}(s) + B_A(\psi)| = 0 \tag{2}$$

where $B_{IC}(s) = 2\pi f C_{IC}(s)$ and $B_A(\psi)$ are the susceptances of the IC and antenna, respectively, ψ is the amount of liquid in direct contact with the antenna. In the case of endoleak, blood flow will promote degradation of the bioresorbable coating, through hydrolysis, and thus alter the boundary condition of the antenna. Consequently, by combining equation (1) with (3) in the linear range $S_{min} \leq s \leq S_{max}$, the sensor code returned by the IC will be:

$$s\left(\psi\right) = \mathrm{nint}\left\{-\frac{1}{C_{step}}\left[C_{IC}\left(S_{min}\right) + \frac{B_A\left(\psi\right)}{2\pi f}\right]\right\}. \tag{3}$$

Potential baselines caused by the device manufacturing process can be eliminated using a *differential sensor code* (Δs) [15]:

$$\Delta s\left(\psi\right) = s\left(0\right) - s\left(\psi\right) \tag{4}$$

where $s\left(0\right)$ is the calibration value obtained from the initial condition of the antenna, i.e. it is fully covered and the degradation process has not yet started.

III. Antenna Design and Simulations

The human abdomen is emulated by a layered rectangular cylinder model (skin, fat, muscle). The abdominal aorta vessel is represented by a cylinder with a sphere (diameter 5.5 cm) to emulate the aneurysm at the implantation depth of 7 cm [16], as shown in Fig. 2. The electrical parameters of the tissues are derived from [17], while coagulated blood from [18]. The

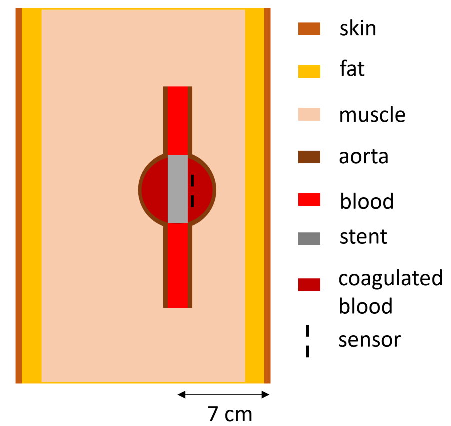

Fig. 2. Stratified electromagnetic model of the human abdomen with an aneurysm of the abdominal aorta.

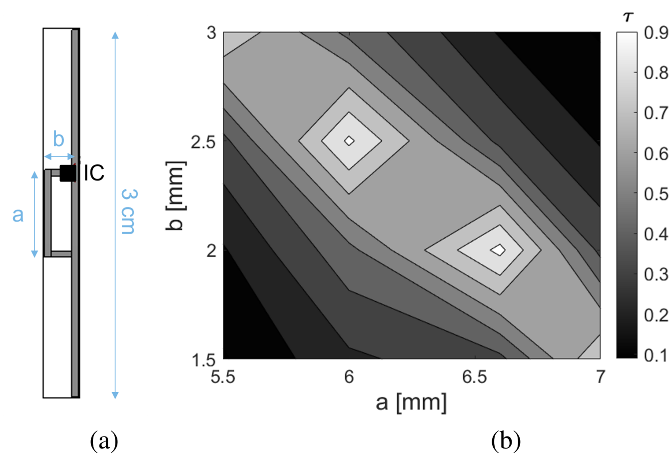

Fig. 3. (a) Geometry of the implanted antenna. (b) Isolines of the power transfer coefficient τ at 900 MHz v.s. geometrical parameters of the Γ-match transformer {a, b}.

stent is emulated by a metallic cylinder with a typical diameter of 2 cm. The antenna selected to be inserted in the aneurysm sac as an RFID sensor to monitor the presence of an endoleak is a dipole (trace width 0.2 mm) equipped with a Γ-match transformer over an FR4 PCB (thickness 0.8 mm, Fig. 3 (a)) and insulation by PolyTetraFluoroEthylene (PTFE). The dipole is placed at a distance of 2 mm from the stent. By fixing the length to 3 cm, the geometrical parameters of the Γ-match are optimized to maximize the power transfer coefficient (τ), i.e. the power collected by the IC at 900 MHz. Fig. 3 (b) shows the isolines of τ at 900 MHz by varying the geometrical parameters $5.5 \leq a \leq 7.0$ mm and $1.5 \leq b \leq 3$ mm. The optimal regions (in white and light gray) are those with $\tau \geq 0.7$. Multiple options are possible; however, the selected configuration is $\{a = 6.6$ mm; $b = 2.0$ mm$\}$ to minimize the footprint.

A. Mid-field Through-The-Body Link

The complete link between the reader antenna and the implanted one is represented as a lossy two-port network [19] which is characterized by the Admittance Matrix $[Y_{i,j}]$ where port 1 (input) and port 2 (output) refer to the terminals of the reader interrogator and the implanted device, respectively. The reader antenna is a linearly polarized microstrip slot as in [9]. The Transducer Power Gain G_T is the main performance metric of the communication link, as it is the ratio between the power supplied by the reader to the IC ($P_{R\rightarrow T}$) and the power available from the generator ($P_{av,R}$). By exploiting the auto-tuning feature of the IC, G_T is defined in terms of admittance as [10]

$$G_T = \frac{P_{R\rightarrow T}}{P_{av,R}} = \frac{4G_G G_{IC}|Y_{12}|^2}{|(Y_{11}+Y_G)(Y_{22}+Y_{IC})-Y_{12}^2|^2} \tag{5}$$

where $Y_G = G_G + jB_G$ is the internal admittance of the reader and $Y_{IC} = G_{IC} + jB_{IC}$ the admittance of the IC. A reliable communication link can be established by providing a communication margin M_{dB}

$$M = G_T + P_{av,R} - P_{IC} - M_0 \geq 0 \tag{6}$$

where $P_{av,R} = 0$ dB is the power emitted by the reader, and $M_{0=3}$ dB is a conservative safe value. In the considered arrangement, the minimum value of G_T to establish the communication is $G_T \geq -40.6$ dB.

The numerical evaluation includes the interaction in the mid-field of the reader antenna with the implanted dipole that when in contact with liquid blood, exposes part of itself to the biological fluid. Fig. 4 (a) reports the considered stages, where starting from stage 0 the antenna is completely coated and electrically insulated and then reaches, in the case of endoleak, stage 3 characterized by a 3.3 mm length of uncovered portion of Γ-match. This is a simulative simplification, however in reality each stage can be identified by areas with different coating thicknesses, and thus controlling its degradation over time when in contact with liquid blood. The corresponding simulated G_T profiles are shown in Fig. 4 (b). Due to the auto-tuning property of the IC, there is a typical nearly flat profile over broadband, comprising the worldwide RFID UHF band. Moreover, the power margin is $M \geq 0$ dB for each stage at 900 MHz, thus the communication link is always verified.

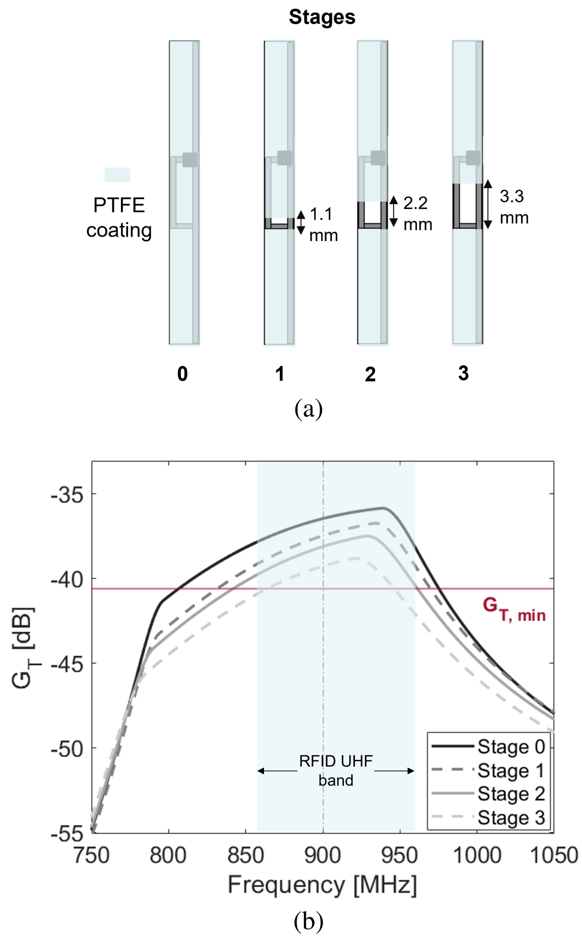

Fig. 4. (a) Sketch of the stages that identify the dissolution of the coating over time, assuming the presence of a bioresorbable material on the Γ-match portion. (b) Simulated Transducer Power Gain G_T for the different stages when the reader antenna interacts in the mid-field.

IV. Prototype and Measurements

The dipole is made with a copper trace (width 0.2 mm) etched with a milling machine over a 0.8 mm thick FR4 substrate, while the IC was mounted using a solder paste (conductive epoxy CW2400 by Chemtronics). The different stages of coating resorption are emulated by varying the coverage made with PTFE, as shown in Fig. 5 (a). The abdomen is emulated by a PET box filled with equivalent liquid of muscle tissue ($\epsilon = 54$; $\sigma = 1.05$ S/m [20]). Each prototype is immersed at a depth of 6 cm from the external reader antenna (Fig. 5 (b)). Electromagnetic characterization is performed by means of the Voyantic Tagformance station in the $800 - 1000$ MHz frequency band. Fig. 5 (c) shows the measured vs. simulated transducer power gain profile over frequency. It is higher than the threshold in the whole RFID UHF band, as expected, and compares well with the simulation, with a difference of less than 3 dB.

To quantify the sensing performance, the different prototypes (one for each stage) are then interrogated by the reader antenna connected to the ThingMagic M6E reader. The measured differential sensor codes, averaged on ten samples [15], are compared with the simulated outcomes in Fig. 6. As expected by the simulations, the differential sensor code increases as the exposed portion of the antenna augments. Nevertheless, the digital contrasts, i.e. the difference of differential sensor codes between different stages, are sharper in the measured cases. Therefore, this device turns out to be a threshold sensor capable of identifying the presence of blood flow around the antenna, since hydrolysis of a hypothetical bioresorbable coating, like a water-soluble polymer hydroxypropylcellulose (HPC), results in the exposure of part of the antenna that increases over time.

V. Conclusion

Numerical analysis and early experiments with a mock-up demonstrated the feasibility of transforming an antenna

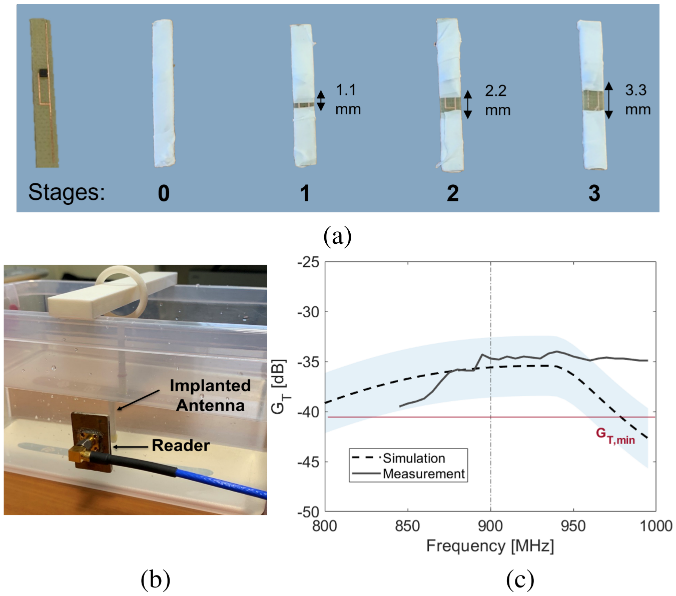

Fig. 5. (a) Realized prototypes for each stage. (b) Measurement setup involving a liquid equivalent of the abdomen. (c) Frequency profile of the simulated and measured Transducer Power Gain G_T of the two-port network that models the mid-field interaction of the implanted antenna (stage 0) and the reader. The ± 3 dB shadow region accounts for manufacturing imperfections.

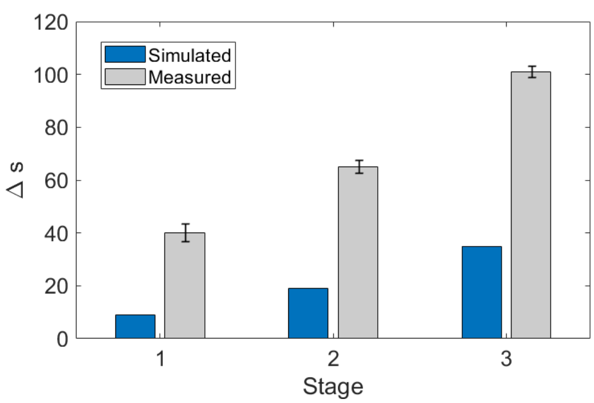

Fig. 6. Comparison between the simulated and measured differential sensor code. The black segments indicate the uncertainties.

into a threshold sensor for the early detection of an endoleak inside the aneurysmatic sac. It is a wireless and batteryless device capable of monitoring the presence of endoleak-related blood flow since it exploits changes in boundary conditions as a result of the hydrolysis of its bioresorbable coating. The digital metric for this application is the differential sensor code returned by a standard RFID query. This feature will be beneficial for the early detection of abnormalities; however, it can be further augmented with a pressure sensor for multi-parametric sensing. Further experiments, including the bioresorbable coating, will be shown during the Conference.

REFERENCES

[1] H. O. Kim, N. Y. Yim, J. K. Kim, Y. J. Kang, and B. C. Lee, “Endovascular aneurysm repair for abdominal aortic aneurysm: a comprehensive review,” *Korean journal of radiology*, vol. 20, no. 8, pp. 1247–1265, 2019.

[2] L. Meuli *et al.*, “Prognostic model for survival of patients with abdominal aortic aneurysms treated with endovascular aneurysm repair,” *Scientific Reports*, vol. 12, no. 1, p. 19540, 2022.

[3] J. Gorich *et al.*, “Leakages after endovascular repair of aortic aneurysms: classification based on findings at ct, angiography, and radiography,” *Radiology*, vol. 213, no. 3, pp. 767–772, 1999.

[4] J. Buth, P. L. Harris, C. van Marrewijk, and G. Fransen, “The significance and management of different types of endoleaks,” in *Seminars in Vascular Surgery*, vol. 16, no. 2. Elsevier, 2003, pp. 95–102.

[5] G. I. Karaolanis *et al.*, “Colour duplex and/or contrast-enhanced ultrasound compared with computed tomography angiography for endoleak detection after endovascular abdominal aortic aneurysm repair: A systematic review and meta-analysis,” *Journal of Clinical Medicine*, vol. 11, no. 13, 2022. [Online]. Available: https://www.mdpi.com/2077-0383/11/13/3628

[6] S. A. A. Shah, Y.-H. Lim, and H. Yoo, “A novel development of endovascular aortic stent system featuring promising antenna characteristics,” *IEEE Transactions on Antennas and Propagation*, vol. 70, no. 3, pp. 2214–2222, 2022.

[7] S. Islam *et al.*, “In vitro study on smart stent for autonomous post-endovascular aneurysm repair surveillance,” *IEEE Access*, vol. 8, pp. 96 340–96 346, 2020.

[8] B. John *et al.*, “Telemetric system for monitoring of endoleak in abdominal aorta aneurysm using multiple pressure sensors integrated on a stent graft,” in *2016 IEEE Biomedical Circuits and Systems Conference (BioCAS)*. IEEE, 2016, pp. 384–387.

[9] F. Naccarata *et al.*, “Wireless and zero-power trans-cardiac link with antennified aortic valve bioprostheses,” *IEEE Journal of Electromagnetics, RF and Microwaves in Medicine and Biology*, pp. 1–9, 2022.

[10] F. Naccarata and G. Marrocco, “Integrated wireless rfid temperature sensor for biological aortic valve prostheses,” *IEEE Journal of Radio Frequency Identification*, pp. 1–1, 2023.

[11] C. Occhiuzzi, G. Contri, and G. Marrocco, “Design of implanted RFID tags for passive sensing of human body: the STENTag,” *IEEE Transactions on Antennas and Propagation*, vol. 60, no. 7, pp. 3146–3154, 2012.

[12] S. Nappi *et al.*, “A fractal-RFID based sensing tattoo for the early detection of cracks in implanted metal prostheses,” *IEEE Journal of Electromagnetics, RF and Microwaves in Medicine and Biology*, 2021.

[13] N. Panunzio *et al.*, “Cyber-tooth: antennified dental implant for RFID wireless temperature monitoring,” in *2021 IEEE International Conference on RFID Technology and Applications (RFID-TA)*. IEEE, 2021, pp. 211–214.

[14] Magnus S3 Axzon, accessed: May. 2, 2022. [Online]. Available: https://axzon.com/rfm3300-d-magnus-s3-m3d-passive-sensor-ic/

[15] F. Naccarata, G. M. Bianco, and G. Marrocco, “Sensing performance of multi-channel RFID-based finger augmentation devices for Tactile Internet,” *IEEE Journal of Radio Frequency Identification*, 2022.

[16] M. R. Skilton *et al.*, “Natural history of atherosclerosis and abdominal aortic intima-media thickness: rationale, evidence, and best practice for detection of atherosclerosis in the young,” *Journal of Clinical Medicine*, vol. 8, no. 8, p. 1201, 2019.

[17] I. Foundation, “Tissue properties database summary,” available online. Accessed: Feb. 1, 2023. [Online]. Available: https://itis.swiss/virtual-population/tissue-properties/database/database-summary/

[18] A. Santorelli, S. Fitzgerald, A. Douglas, K. Doyle, and M. O’Halloran, “Dielectric profile of blood clots to inform ischemic stroke treatments,” in *2020 42nd Annual International Conference of the IEEE Engineering in Medicine & Biology Society (EMBC)*. IEEE, 2020, pp. 3723–3726.

[19] S. J. Orfanidis, *Electromagnetic Waves and Antennas*. [Online]. Available: http://eceweb1.rutgers.edu/ orfanidi/ewa/

[20] Speag Swiss, accessed: May. 5, 2022. [Online]. Available: https://speag.swiss/components/materials-liquids/msl/